Title

Metal—Metal-Bonded Fe4 Clusters with Slow Magnetic Relaxation

Journal

Inorganic Chemistry, 61(26)

ISSN

0020-1669

Authors

Hertler, Phoebe R

Kautzsch, Linus

Touchton, Alexander J

et al.

Publication Date

2022-07-04

DOI

10.1021/acs.inorgchem.2c00865

Metal-metal Bonded Fe_4 Clusters with Slow Magnetic Relaxation

Phoebe R. Hertler[a], Linus Kautzsch[b], Alexander J. Touchton[a], Guang Wu[a], and Trevor W. Hayton*[a]

[a] *Department of Chemistry and Biochemistry, University of California Santa Barbara, CA 93106*

[b] *Materials Department and Materials Research Laboratory, University of California, Santa Barbara, CA 93106*

*To whom correspondence should be addressed. Email: hayton@chem.ucsb.edu

Abstract

Reaction of $FeBr_2$ with $Li(N{=}C^tBu_2)$ (0.5 equiv) and Zn^0 (2 equiv) results in the formation of the formally mixed-valent cluster $[Fe_4Br_2(N{=}C^tBu_2)_4]$ (**1**) in moderate yield. Subsequent reaction of **1** with $Na(N{=}C^tBu_2)$ results in formation of $[Fe_4Br(N{=}C^tBu_2)_5]$ (**2**), also in moderate yield. Both **1** and **2** were characterized by zero-field ^{57}Fe Mössbauer spectroscopy, X-ray crystallography, and SQUID magnetometry. Their tetrahedral $[Fe_4]^{6+}$ cores feature short Fe-Fe interactions (ca. 2.50 Å). Additionally, both **1** and **2** display S = 7 ground states at room temperature and slow magnetic relaxation with zero-field relaxation barriers of U_{eff} = 14.7(4) and 15.6(7) cm^{-1}, respectively. Moreover, AC magnetic susceptibility measurements were well modelled by assuming an Orbach relaxation process.

Introduction

Transition metal clusters featuring direct metal-metal orbital overlap are emerging as a new class of single molecule magnets (SMMs).[1,2] The metal-metal bonding present in these clusters can result in ferromagnetic (direct) exchange interactions and energetically isolated magnetic ground states,[3–11] often leading to complexes with high relaxation barriers and long lived magnetization.[1,12–19] For example, $[Bu_4N][(^{H}L)_2Fe_6(py)_2]$ ($^{H}LH_6$ = $MeC(CH_2NHPh\text{-}o\text{-}NH_2)_3$) features an S = 19/2 ground state and a relaxation barrier of U_{eff} = 42.5(8) cm^{-1}.[3] This cluster exhibits an octahedral arrangement of six Fe atoms, with relatively short Fe-Fe bonds (ca. 2.61 Å), and its magnetic properties are thought to be a consequence of its well-isolated, giant-spin ground state, which suppresses magnetization tunneling. Similarly, $[Co_4(N{=}P^tBu_3)_4]^+$ exhibits a giant-spin S = 9/2 ground state with U_{eff} = 87 cm^{-1}.[12] Like $[Bu_4N][(^{H}L)_2Fe_6(py)_2]$, this cluster features a compact metal core with short Co-Co bonds (2.36 Å), which leads to slow magnetic relaxation. The Fe(II) chain clusters $[Fe_4(tpda)_3X_2]$ (H_2tpda = *N*,*N*-bis(pyridin-2-yl)pyridine-2,6-diamine; X = Cl, Br) and $[Fe_3(DpyF)_4][BF_4]_2$ (DpyF = dipyridylformamide) also exhibit ferromagnetic exchange and slow magnetic relaxation,[19–21] although in these examples the Fe-Fe distances are relatively long (>2.8 Å). Several other Fe-Fe bonded complexes also feature high spin ground states as a consequence of direct exchange interactions, including $[Na_6Fe_3$(tris-*cyclo*-salophen)$(py)_9]$,[4] $[Fe(^{i}PrNPPh_2)_3Fe(PMe_3)]$,[5] $[Fe_2(DPhF)_3]$, and $[Fe_2(DPhF)_4]$ (DPhF = diphenylforamidinate).[22–25] While the magnetic relaxation in these examples was not explicitly measured, the observation that direct M-M bonding can lead to ferromagnetic exchange further highlights the value of this design feature.

Recently, we reported the synthesis and characterization of the ketimide-supported Fe_4 cluster, $[Fe_4(N{=}CPh_2)_6]$.[13] This complex features relatively short Fe-Fe bonds within its tetrahedral

Fe_4 core and an $S = 7$ ground state that persists at room temperature. Additionally, it exhibits good SMM properties, including a relaxation barrier of $U_{eff} = 29$ cm^{-1} and relatively long relaxation times (up to $t = 34$ s at $T = 1.8$ K). More remarkably, we observe no evidence for through-barrier relaxation in its AC relaxation measurements. We hypothesized that its good SMM performance was due to direct exchange-mediated ferromagnetic coupling amongst the four Fe centers, which was promoted by the ketimide group. In fact, the ketimide ligand is known for its ability to promote both metal-metal bonding and magnetic communication, as shown by the isolation of the $[Cu(N{=}C^tBu_2)]_4$, which is stabilized by cuprophilic interactions,[26] and $[Pd_7(N{=}C^tBu_2)_6]$,[27] which features an unusual hexagonal planar Pd_7 core. Also notable are the bimetallic ketimide complexes, $[Li(12\text{-crown-}4)_2][M_2(N{=}C^tBu_2)_5]$ (M = Mn, Fe, Co),[28] $[Fe_2(N{=}C^tBu_2)_5]$,[28] and $[Li][Cr_2(N{=}C_{10}H_{14})_7]$,[29] which feature varying degrees of magnetic communication as assayed by SQUID magnetometry.

In an effort to test the effect of the ketimide substituents on the magnetic properties of $[Fe_4(N{=}CPh_2)_6]$, we endeavored to synthesize an Fe_4 cluster supported by the bis(*tert*-butyl) ketimide ligand, which has much different electronic and steric properties than the di(phenyl) ketimide ligand employed previously. Herein, we report the synthesis and magnetic characterization of $[Fe_4Br_2(N{=}C^tBu_2)_4]$ and $[Fe_4Br(N{=}C^tBu_2)_5]$. Despite having fairly short relaxation times, these complexes show no evidence of relaxation by quantum tunneling, cementing the role that direct-exchange interactions can play in generating SMMs.

Results and Discussion

In an effort to synthesize $[Fe_4(N{=}C^tBu_2)_6]$, we applied the same synthetic protocol used to generate $[Fe_4(N{=}CPh_2)_6]$.[13] Thus, reaction of $FeBr_2$ with 1.5 equiv of $Li(N{=}C^tBu_2)$ and 2 equiv of Zn powder in THF at room temperature for 18 h results in the self-assembly of $[Fe_4Br_2(N{=}C^tBu_2)_4]$

(**1**), which could be isolated as deep purple blocks in low yield. Complex **1** is also formed using the rational stoichiometry of 1 equiv of $FeBr_2$ and 1 equiv of $Li(N{=}C^tBu_2)$; however, the highest yields were achieved upon reaction of $FeBr_2$ with 0.5 equiv of $Li(N{=}C^tBu_2)$ and 2 equiv of Zn powder in THF at room temperature for 18 h, which provided **1** in 45% yield (based on $Li(N{=}C^tBu_2)$) after work-up (Scheme 1). Curiously, complex **1** is still formed, albeit in low yields, when excess $Li(N{=}C^tBu_2)$ (up to 2 equiv per $FeBr_2$) is employed in the reaction, suggesting that its two bromide ligands are relatively resistant to salt metathesis. Treatment of other ferrous salts (e.g., $FeCl_2$, FeI_2, $Fe(OAc)_2$) with $Li(N{=}C^tBu_2)$ (1.5 equiv) and Zn^0 (2 equiv) also failed to generate the desired $[Fe_4(N{=}C^tBu_2)_6]$.

As a solid, **1** is stable under an inert atmosphere at -25 °C for several months. However, it rapidly decomposes on exposure to air, in both the solid state and solution. Complex **1** is slightly soluble in pentane, and very soluble in Et_2O, THF, benzene, and CH_2Cl_2. It is insoluble in acetonitrile and decomposes on dissolution in pyridine. Its ^1H NMR spectrum in C_6D_6 features a broad resonance at 120.8 ppm assignable to the single ^{t}Bu environment (Figure S2), consistent with the idealized D_{2d} symmetry observed in the solid state (see below).

Scheme 1. Synthesis of Complexes **1** and **2**

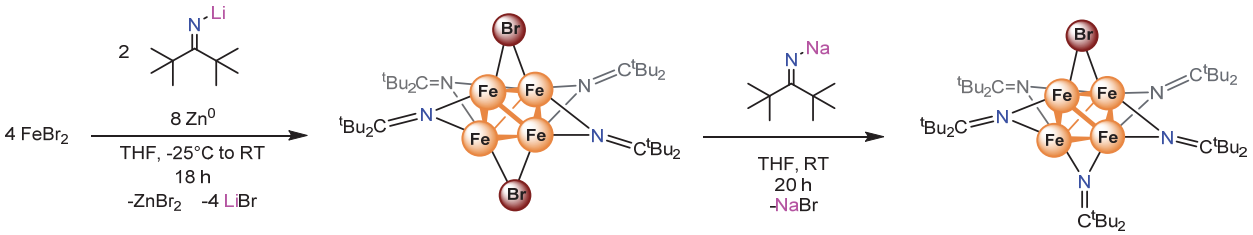

Complex **1** crystallizes in the monoclinic space group $P2_1/c$ (Figure 1). Its solid-state molecular structure reveals a tetrahedral $[Fe_4]^{6+}$ core, wherein four edges are bridged by μ-$N{=}C^tBu_2$ ligands and two are bridged μ-bromide ligands. The two bromide ligands feature *trans* stereochemistry,

generating a complex with idealized D_{2d} symmetry. The average Fe–Fe distance is 2.50 Å (range = 2.4193(9) – 2.5510(9) Å; Table 1), which corresponds to a formal shortness ratio of r = 1.07, suggesting the presence of weak single bonds between the Fe centers.[30,31] The Fe-Fe bonds in **1** are slightly shorter than the Fe–Fe bonds reported for $[Fe_4(N{=}CPh_2)_6]$ (average = 2.56 Å; r = 1.10; range = 2.504(4) – 2.621(4) Å),[13] suggesting that the bis(*tert*-butyl)ketimide ligands does promote stronger metal-metal bonding than the di(phenyl)ketimide; however, these shorter bonds do not result in better SMM performance (see below). For further comparison, its Fe-Fe distances are similar to the Fe-Fe distances in $[Fe_2(N{=}C^tBu_2)_5]^-$ (2.443(1) Å; r = 1.05) and $[Fe_4(\mu\text{-}C_6H_4\text{-}4\text{-}Me)_6(THF)_4]$ (average = 2.47 Å; r = 1.06).[22,28,32] Finally, the average Fe–Br distance in **1** is 2.51 Å (range = 2.4937(8) – 2.5331(8) Å) and the average Fe-N distance is 1.98 Å. The latter parameter compares well to the average Fe-N distance in $[Fe_4(N{=}CPh_2)_6]$ (1.95 Å).[13]

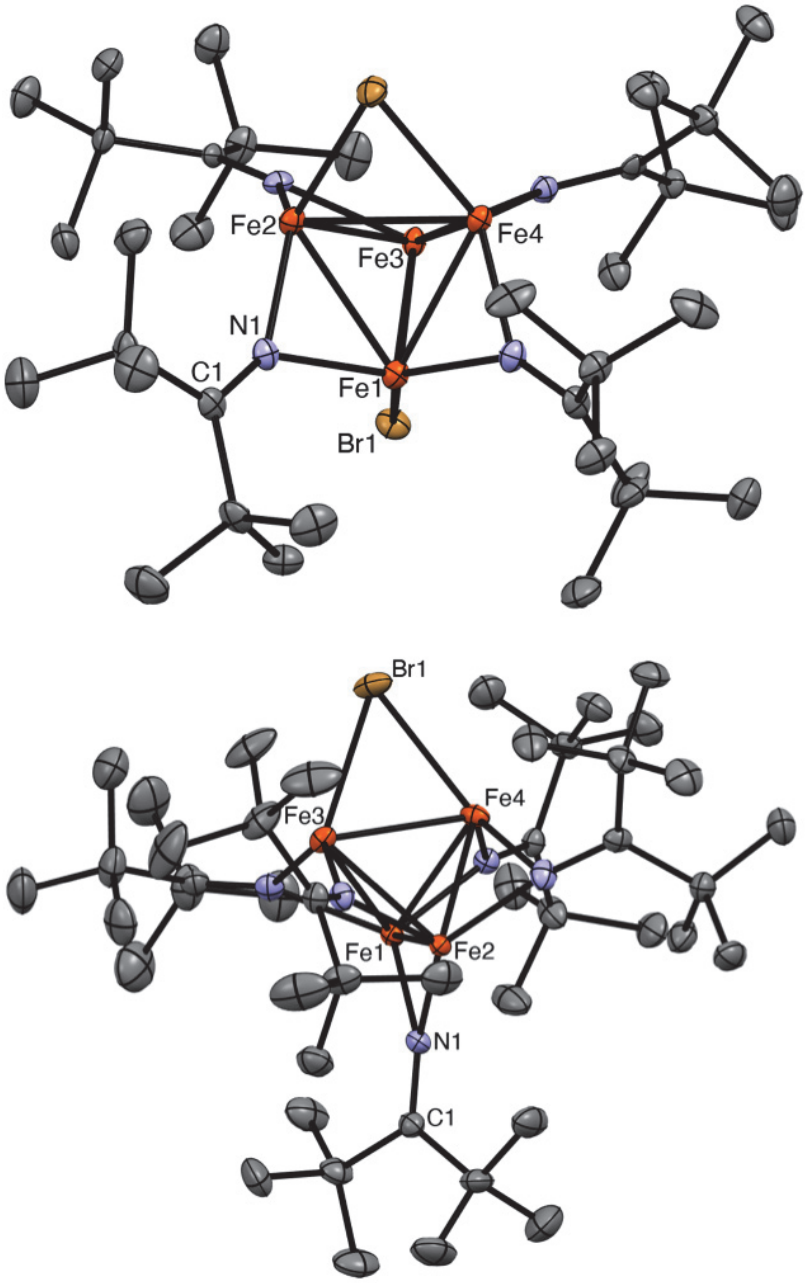

Figure 1. Solid-state molecular structures of **1** (top) and **2** (bottom), shown with 50% probability ellipsoids. Hydrogen atoms and alternate position of the Fe_4 core in **2** are omitted for clarity.

Table 1. Selected bond lengths (Å) and angles (°) for complexes **1** and **2**.

Complex	**1**	**2**
Fe–Fe	2.4856(9) 2.5293(9) 2.4193(9)	2.5238(6) 2.5648(6) 2.4376(6)

	2.5510(9) 2.5296(9) 2.4736(8)	2.4651(6) 2.4525(6) 2.4658(7)
Fe–N	1.962(3) 1.982(3) 1.998(3) 1.999(3) 1.982(3) 1.990(3) 1.964(3) 1.969(3)	1.996(2) 2.012(2) 1.990(2) 2.004(2) 2.025(2) 1.897(2) 1.975(2) 1.953(2) 1.979(2) 2.015(2)
Fe–Br	2.5331(8) 2.4974(7) 2.4937(8) 2.5085(7)	2.5213(5) 2.5271(5)
C=N	1.278(5) 1.260(5) 1.268(5) 1.264(5)	1.265(3) 1.268(3) 1.271(3) 1.273(3) 1.270(3)
Fe–N–Fe	78.07(13) 75.14(12) 77.27(13) 79.92(12)	78.06(7) 76.57(8) 80.27(8) 77.58(8) 75.77(7)
Fe–Br–Fe	60.75(2) 60.36(2)	58.474(16)

In an effort to replace the two bromide ligands in **1** with ketimide moieties, we studied the reactivity of **1** with other ketimide sources. Thus, reaction of **1** with 2 equiv of Na(N=C^{t}Bu$_2$) in THF for 20 h at room temperature results in formation of [Fe$_4$Br(N=C^{t}Bu$_2$)$_5$] (**2**), which could be isolated in low yield after work-up. Complex **2** could be isolated in better yields upon reaction of **1** with only 1 equiv of Na(N=C^{t}Bu$_2$) in THF (Scheme 1). Under these conditions, **2** can be isolated in 49% yield as deep red-black needles. Surprisingly, even with heating and longer reaction times, metathesis of the final bromide ligand could not be achieved. Additionally, reaction of **1** with 2

equiv of Li(N=C^{t}Bu$_2$) only resulted in formation of the previously reported monometallic Fe(II) complex, [Li(THF)]$_2$[Fe(N=C^{t}Bu$_2$)$_4$],[33] as assayed by ^{1}H NMR spectroscopy (Figure S3).

The ^{1}H NMR spectrum of **2** in C_6D_6 features broad resonances at 98 ppm and 79 ppm, which are assignable to the methyl groups of the equatorial and axial ketimide ligands, respectively (Figure S4). The ESI-MS of **2**, recorded in THF in the positive ion mode, features a major peak at 1003.3074 *m/z*, corresponding to [Fe$_4$Br(N=C^{t}Bu$_2$)$_5$]$^+$ (calcd 1003.3762 *m/z*) (Figures S11-S12), further confirming its formulation.

Complex **2** crystallizes in the monoclinic space group $P2_1/c$ (Figure 1). Its solid-state molecular structure reveals a tetrahedral Fe$_4$ core ligated by one μ-bromide ligand and by five μ-ketimide ligands, generating a complex with idealized C_{2v} symmetry. The [Fe$_4$]$^{6+}$ core is disordered over two sites, which were modelled in 90:10 ratio; however, there is no apparent disorder of either the bromide or ketimide ligands. The average Fe–Fe distance is 2.48 Å (range = 2.4376(6) – 2.5648(6) Å) (Table 1), which corresponds to a formal shortness ratio of r = 1.06.[30,31] This value is comparable to that found in **1**, and is indicative of the presence of weak Fe-Fe bonding. The Fe-Br and Fe-N distances in **2** are also comparable to those found in complex **1**.

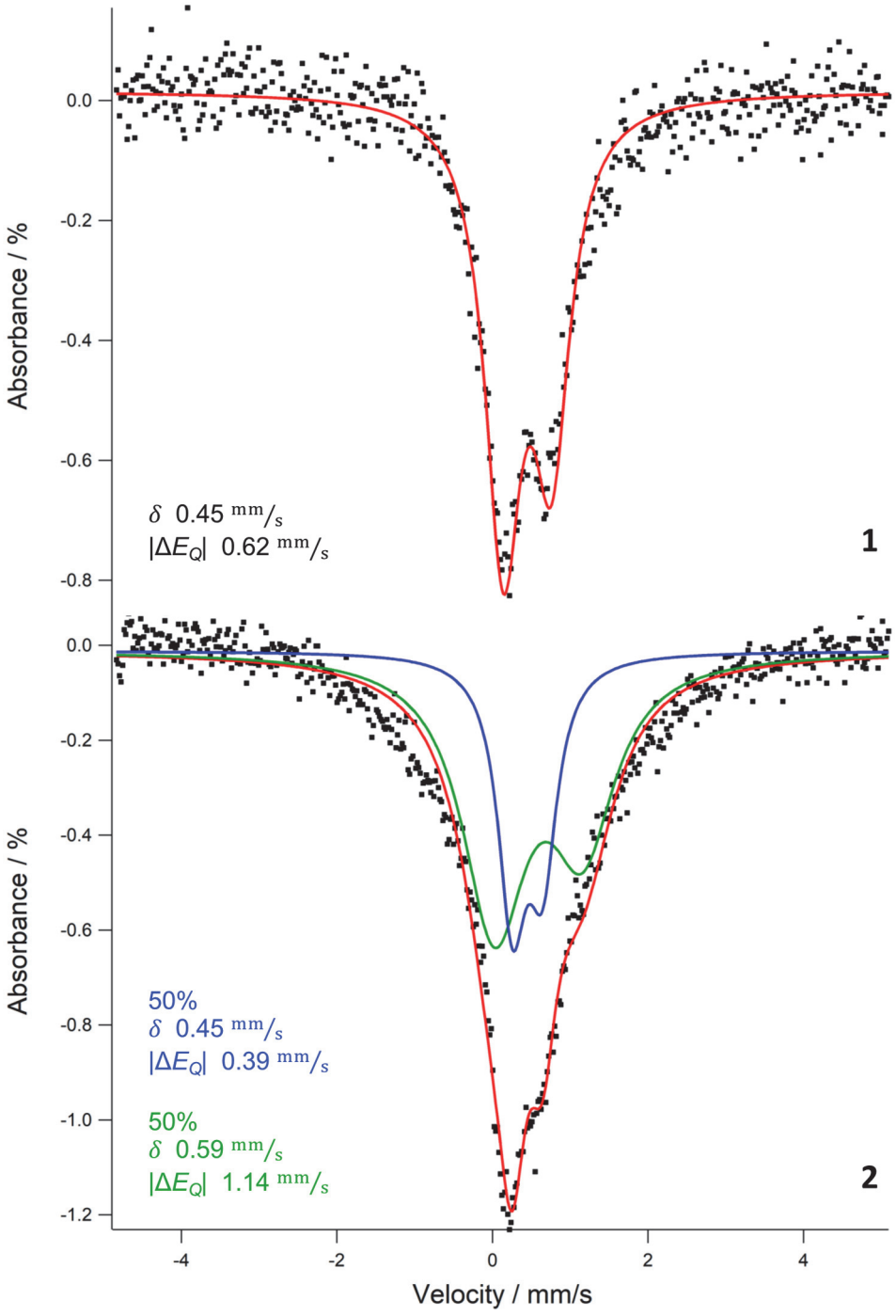

Figure 2. Zero-field ^{57}Fe Mössbauer spectra of **1** (top) and **2** (bottom) collected at $T = 90$ K. The red traces correspond to the overall fit, while the blue and green traces correspond to the two doublets employed to fit **2**.

The ^{57}Fe Mössbauer spectrum of **1** taken at T = 90 K reveals a single asymmetric doublet indicative of a single iron environment (Figure 2), consistent with the idealized D_{2d} symmetry of the complex, which should result in a single Fe environment. The doublet has an isomer shift of δ = 0.45 mm/s and a quadrupole splitting of $|\Delta E_Q|$ = 0.62 mm/s. For **2**, the zero-field ^{57}Fe Mössbauer spectrum at T = 90 K displays a broad signal consistent with two overlapping asymmetric doublets. One doublet has an isomer shift of δ = 0.45 mm/s and a quadrupole splitting of $|\Delta E_Q|$ = 0.39 mm/s, whereas the second doublet has an isomer shift of δ = 0.59 mm/s and a quadrupole splitting of $|\Delta E_Q|$ = 1.14 mm/s. The spectrum is consistent with the idealized C_{2v} symmetry of the complex, which should result in two different Fe environments in a 1:1 ratio. These spectra are similar to those reported for other Fe(I)/Fe(II) mixed-valent clusters. For example, the mixed-valent Fe(I)/Fe(II) species [MgCl(THF)$_5$][Fe$_8$Me$_{12}$] exhibits a broad doublet with an isomer shift of δ = 0.30 mm/s and a quadrupole splitting of ΔE_Q = 0.85 mm/s,[34] [Fe$_4$(μ-Ph)$_6$(THF)$_4$] features parameters of δ = 0.6 and $|\Delta E_Q|$ = 0.84 mm/s, and [Fe$_4$(N=CPh$_2$)$_6$] features parameters of δ = 0.34 mm/s and $|\Delta E_Q|$ = 0.79 mm/s.[13,32] The UV-vis-NIR spectrum of **1** in THF at 298 K (Figure S7) exhibits a broad absorption band at 827 nm (ε = 1200 L mol^{-1} cm^{-1}), which we tentatively assign to an intervalence charge transfer (IVCT). Similarly, the UV-vis-NIR spectrum of **2** in THF at 298 K (Figure S8) exhibits a broad band at 923 nm (ε = 1100 L mol^{-1} cm^{-1}). The appearance of IVCT bands for both complexes is evidence for electron delocalized Class II- or Class III-type behavior,[7,35–37] and is consistent with our Mössbauer results.

Temperature-dependent dc magnetization data were collected for a crystalline sample of **1** at H = 5000 Oe, revealing a μ_{eff} value of 16.18 μ_B at T = 300 K ($\chi_M T$ = 32.73 cm^{3}K/mol), which corresponds to an S = 7 ground state (Figure 3a). Similarly, the magnetic susceptibility of **2**, under the same applied field, was found to be μ_{eff} = 16.15 μ_B at T = 300 K ($\chi_M T$ = 32.61 cm^{3}K/mol). The

related $[Fe_4]^{6+}$ cluster, $[Fe_4(N{=}CPh_2)_6]$ features a comparable moment (μ_{eff} = 14.64 μ_B at T = 300 K),[13] suggesting the same S = 7 ground state for all three complexes. Importantly, these room temperature moments imply strong spin delocalization across the $[Fe_4]^{6+}$ core. For comparison, a cluster with discrete Fe(I) and Fe(II) centers would exhibit a μ_{eff} value of 8.83 μ_B.[13] We hypothesize that the ferromagnetic coupling observed in **1** and **2** is due to direct exchange; however, double exchange has also been used to explain ferromagnetic coupling in formally mixed-valent bimetallic iron complexes,[38,39] and it could be operative here, as well.

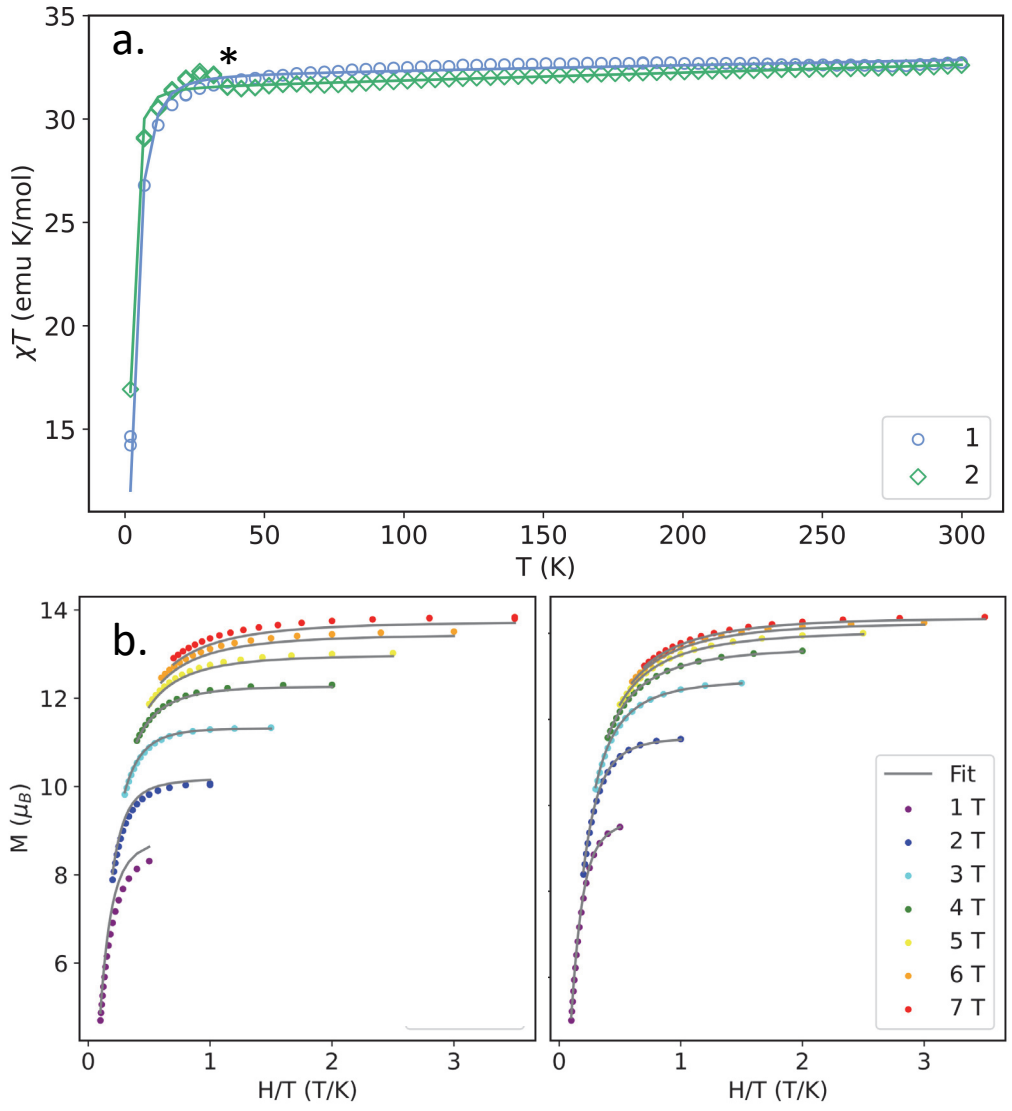

Figure 3. a. Magnetic susceptibility multiplied by temperature ($\chi_M T$) for **1** (blue circles) and **2** (green diamonds) collected under an applied magnetic field of $H = 5$ kOe from $T = 2$ K to $T = 300$ K. The solid lines represent fits to the spin Hamiltonian $\widehat{H} = D\hat{S}_z^2 + g_{iso}\mu_B SH$, where $S = 7$, $D = -0.85$ cm^{-1}, $\chi_{TIP} = 0.0026$ cm^3 mol^{-1}, and $g = 2.14$ for **1**, and $S = 7$, $D = -0.14$ cm^{-1}, $\chi_{TIP} = 0.0038$ cm^3 mol^{-1}, and $g = 2.12$ for **2**. The asterisk indicates the antiferromagnetic transition of O_2. b. Variable-temperature, variable-field reduced magnetization data for **1** (left) and **2** (right). Data was collected at temperatures ranging from $T = 2$ to $T = 10$ K. Gray lines represent fits to the data, as described in the main text.

Variable-temperature, variable-field (VTVF) reduced magnetization data for **1** and **2** both feature non-superimposable isocurves (Figure 3b), indicative of slow magnetic relaxation, as was observed for [$Fe_4(N{=}CPh_2)_6$].[13] The VTVF data were fit with the PHI software package according to the spin Hamiltonian $\widehat{H} = D\hat{S}_z^2 + E\left(\hat{S}_x^2 - \hat{S}_y^2\right) + g_{iso}\mu_B SH$, to give $D = -0.41$ cm^{-1}, $|E/D| = 0.002$, and $g = 2.07$ for **1**, and $D = -0.27$ cm^{-1}, $|E/D| = 0.02$, and $g = 2.09$ for **2** (Figure 3b).[40] These parameters are comparable to those observed for [$Fe_4(N{=}CPh_2)_6$], which exhibited values of $D = -0.75$ cm^{-1}, $|E/D| = 0.17$, and $g = 1.92$.[13]

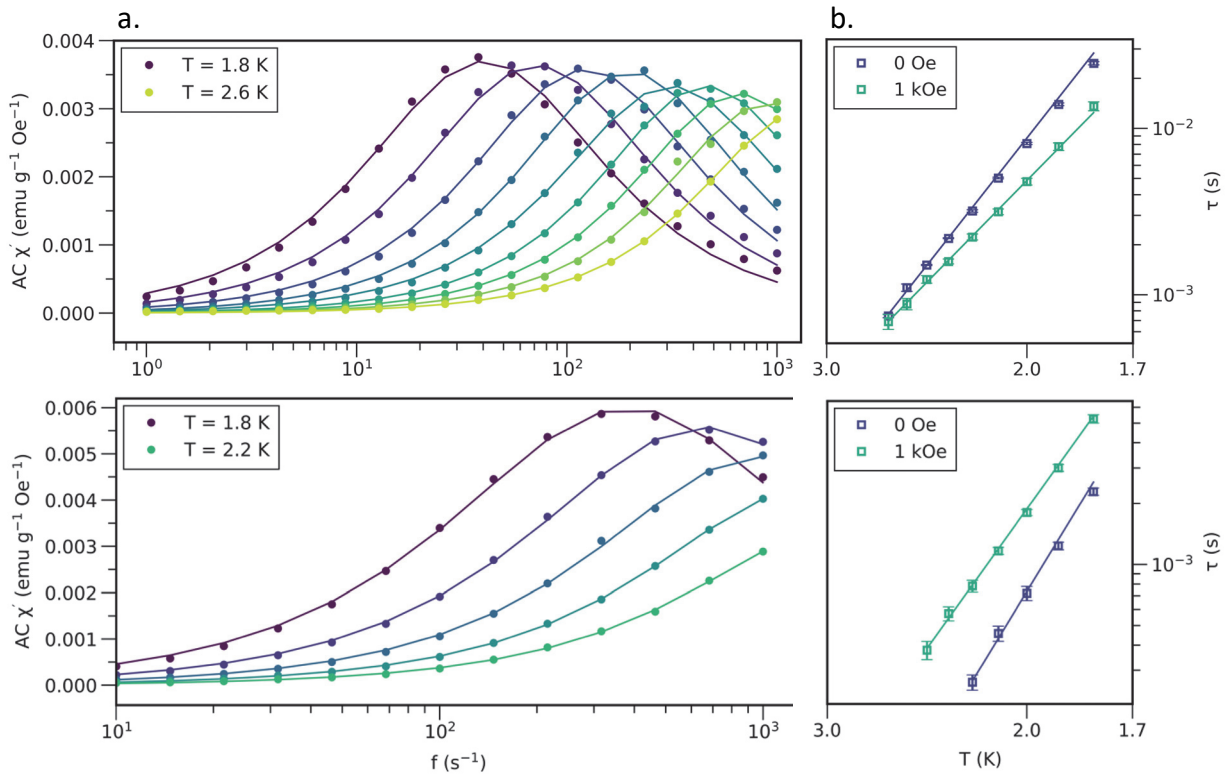

Figure 4. (a) Imaginary part of the AC susceptibility of **1** (top) and **2** (bottom) at zero field as a function of excitation frequency and temperature. The temperature was increased by 0.1 K increments between isotherms. The lines shown are fits to the generalized Debye model. (b) Arrhenius plot of the relaxation times of **1** (top) and **2** (bottom) in zero field (navy) and under H = 1 kOe applied field (teal). The fits shown are to eq 1.

Magnetic hysteresis measurements show waist-restricted $M(H)$ hysteresis loops at T = 2 K for both **1** and **2** (Figures S16 and S22), suggesting rapid relaxation of the magnetization when H approaches 0 Oe. To probe the mechanism(s) of magnetic relaxation, the relaxation dynamics of **1** and **2** were measured with ac magnetic susceptibility measurements. Data were recorded at H = 0 and H = 1000 Oe applied fields at temperatures between T = 1.8 K and T = 2.6 K and frequencies

between f_{ac} = 1 Hz and f_{ac} = 1000 Hz. For both **1** and **2**, the in-phase (χ_M') and out-of-phase (χ_M") measurements were fit using a generalized Debye model, and relaxation times (τ) were extracted from these fits (Figure 4). A corresponding plot of ln(τ) versus T^{-1} is linear for both complexes under both zero field and H = 1000 Oe applied field, consistent with an Orbach relaxation process, as described by the equation:

$$\tau^{-1} = \tau_0^{-1} \exp\left(-\frac{U_{eff}}{k_B T}\right) \quad \textbf{(1)}$$

Where τ is the observed relaxation time, U_{eff} is the effective spin-reversal barrier, k_B is the Boltzmann constant, and τ_0 is a pre-exponential factor. That said, we cannot exclude the possibility that Raman relaxation is also operative, given the narrow temperature range of our ac data.

Applying eq 1 to the relaxation data recorded for complex **1** at H = 0 Oe and H = 1000 Oe yields τ_0 values of 2.2(5) × 10^{-7} s and 1.0(1) × 10^{-6} s, and U_{eff} values of 14.7(4) cm^{-1} and 11.8(2) cm^{-1}, respectively. The relaxation data for **2** at H = 0 Oe and H = 1000 Oe could also be fit to eq 1, yielding τ_0 values of 1.0(5) × 10^{-8} s and 1.4(4) × 10^{-7} s, and U_{eff} values of 15.6(7) cm^{-1} and 13.2(4) cm^{-1}, respectively. The values of U_{eff} calculated for **1** and **2** using $U = |D|S^2$ are U = 20.1 cm^{-1} and 13.2 cm^{-1}, respectively. The latter is in good agreement with that determined from the ac magnetic susceptibility measurements, but the former is larger, suggesting that Raman relaxation may also be occurring in this complex, which lowers the effective barrier.[12] For comparison, $[Fe_4(N{=}CPh_2)_6]$ features a U_{eff} value of 29.1(1) cm^{-1},[13] whereas the tetrametallic SMMs $[Ni_4(N{=}P^tBu_3)_4][B(C_6F_5)_4]$ and $[Co_4(N{=}P^tBu_3)_4][B(C_6F_5)_4]$ feature U_{eff} values of 16.53(6) cm^{-1} and 87 cm^{-1}, respectively.[2,12] While it is difficult to extract structure-function relationships from this small series of complexes, it is heartening to observe that they universally exhibit slow magnetic relaxation, strengthening the argument that direct exchange will be an important criterion for the design of high-performing SMM in the years to come.

Conclusions

In summary, we report the synthesis of $[Fe_4Br_2(N{=}C^tBu_2)_4]$ and $[Fe_4Br(N{=}C^tBu_2)_5]$, two ketimide-supported $[Fe_4]^{6+}$ clusters. Both clusters exhibit $S = 7$ ground states at room temperature, which results from strong ferromagnetic coupling between the Fe(I) and Fe(II) centers within the $[Fe_4]^{6+}$ core. Additionally, both clusters exhibit slow magnetic relaxation with zero-field relaxation barriers of $U_{eff} \approx 14$ cm^{-1}. While their barriers to magnetic relaxation are modest, we observe no evidence for relaxation via quantum tunneling, bolstering the use of ferromagnetic direct exchange to generate new, high-performing SMMs.[41] Additionally, this work highlights the utility of the ketimide ligand to generate metal clusters with significant amounts of direct M-M bonding.

Experimental Details

General Procedures. All operations were performed in a glovebox under an atmosphere of N_2. Diethyl ether (Et_2O) was dried by passage over activated molecular sieves using a Vacuum Atmospheres DRI-SOLV solvent purification system. Tetrahydrofuran (THF) was distilled over Na/benzophenone and stored over activated 3 Å molecular sieves for 24 h prior to use. Acetonitrile was stored over activated 3 Å molecular sieves for three days and degassed by sparging with N_2 prior to use. Pentane was dried on an MBraun solvent purification system. C_6D_6 and ^{t}BuCN were dried over activated 3 Å molecular sieves for 72 h prior to use. $FeCl_2$ was purchased from Strem and stirred in a mixture of diethyl ether and TMSCl for 18 h at room temperature prior to use. $Li(N{=}C^tBu_2)$ was prepared according to published literature procedures.[42] All other reagents were purchased from commercial suppliers and used as received.

All NMR spectra were collected at room temperature. ^{1}H NMR spectra were recorded on an Agilent Technologies 400-MR DD2 400 MHz or a Varian Unity Inova 500 MHz spectrometer. NMR spectra were referenced to external $SiMe_4$ using residual solvent resonances as internal standards. Electronic absorption spectra were recorded on a PerkinElmer Lambda 750 UV/Vis/NIR Spectrophotometer. IR spectra were recorded on a Nicolet 6700 FT-IR spectrometer with a NXR FT Raman Module. Mass spectra were collected at the Materials Research Laboratory Shared Experimental Facilities at UCSB, using an electrospray ionization (ESI) source in positive ion mode with a Waters Xevo G2-XS TOF Time-of-Flight mass spectrometer. Model mass spectra were generated in MassLynx V4.1 software with the isotope clusters displayed with a minimum abundance of 0.1%. Elemental analyses were performed by the Microanalytical Laboratory at the University of California, Berkeley, using a Perkin Elmer 2400 Series II combustion analyzer.

Zero-Field ^{57}Fe Mössbauer Spectroscopy. Data were collected on a SEECo Model W304 resonant gamma-ray spectrometer (activity = 50 mCi ± 10%), ^{57}Co/Rh source (manufactured by Ritverc) equipped with a Janis Research Model SVT-400 cryostat system. The source linewidth is <0.12 mm/s for the outermost lines of a 25 micron α-Fe foil standard. Isomer shifts are referenced to a α-Fe foil at room temperature. ^{57}Fe Mössbauer samples were prepared using 35 mg of crystalline **1** and 21 mg of crystalline **2** suspended in Paratone-N oil and measured at 90 K. The samples were loaded into a polypropylene capsule under inert atmosphere, which was subsequently sealed with vacuum grease to prevent exposure to air. The data were fit using a custom Igor Pro (Wavemetrics) macro package developed by the Betley group at Harvard University.

Magnetic Measurements. Magnetic properties were recorded using a Quantum Design Magnetic Property Measurement System SQUID vibrating sample magnetometer (MPMS3 SQUID-VSM).

15-25 mg samples of polycrystalline material were loaded into a glass NMR tube, which was subsequently flame sealed under static vacuum. For **1**, the solids were kept in place by adding eicosane wax (37 mg), which was subsequently melted into the sample to minimize torqueing during measurements. For **2**, the solids were kept in place by quartz wool packed on either side of the sample. DC magnetic measurements were performed in VSM mode while sweeping either the applied magnetic field or temperature at controlled rates. Variable-temperature, variable-field magnetization data was collected under fields ranging from $H = 1$ to $H = 7$ T over the temperature range 2 to 20 K. The data was fitted using the program PHI.[40] AC susceptibility measurements were performed at fixed temperatures and fields in three-point measurement mode with an excitation field amplitude of 2 Oe. AC susceptibility data was fit using the generalized Debye model. For the magnetic susceptibility measurements, diamagnetic corrections ($\chi_{dia} = -5.37\times10^{-4}$ cm^3/mol for $[Fe_4Br_2(N{=}C^tBu_2)_4]$, $\chi_{dia} = -6.07\times10^{-4}$ cm^3/mol for $[Fe_4Br(N{=}C^tBu_2)_5]$) were made using Pascal's constants.[43] The data was not corrected for the contributions from the sample holder, quartz wool, or eicosane.

Synthesis of $[Fe_4Br_2(N{=}C^tBu_2)_4]$ (1). To a cold (-25 °C), stirring suspension of $FeBr_2$ (0.402 g, 1.86 mmol) in THF (3 mL) was added dropwise a cold solution of $Li(N{=}C^tBu_2)$ (0.139 g, 0.94 mmol) in THF (5 mL), which resulted in a color change to deep red-brown. The reaction mixture was allowed to warm to room temperature, whereupon Zn^0 powder (0.245 g, 3.74 mmol) was added, which resulted in a slow color change to deep purple-red. After 18 h, the volatiles were removed *in vacuo* resulting in formation of a deep purple solid. The solid was triturated with pentane (6 × 1 mL), extracted with pentane (10 mL), and filtered through a Celite column supported on glass wool (0.5 cm × 5 cm). The filtrate was concentrated *in vacuo* and transferred to a 5 mL vial, which was placed inside of a 20 mL scintillation vial. Isooctane (2 mL) was added

to the outer vial. Storage of this two-vial system at -25 °C for 48 h resulted in the deposition of large black-purple blocks. The crystalline material was isolated by decanting the supernatant and then washed with cold (-25 °C) pentane (2 × 1 mL). The washings were discarded and the crystals were dried *in vacuo*, yielding **1** (100 mg, 45% yield). Anal. Calcd for $C_{36}H_{72}Br_2Fe_4N_4$: C 45.80, H 7.69, N 5.93%. Found: C 45.62, H 7.52, N 5.82%. ^{1}H NMR (400 MHz, 25 °C, C_6D_6): δ 120.8 (br s, 72 H). UV-vis/NIR (THF, 0.10 mM, 25 °C, L mol^{-1} cm^{-1}): 527 nm (ε = 3700), 827 nm (ε = 1200). FT-IR (KBr pellet, cm^{-1}): 586 (s), 640 (s), 763 (m), 837 (m), 871 (w), 964 (s), 1037 (m), 1105 (w), 1141 (w), 1193 (s), 1209 (s), 1228 (m), 1361 (s), 1371 (s), 1400 (m), 1459 (m), 1479 (s), 1554 (m), 1575 (s), 1587 (m), 1648 (m), 1672 (w), 2233 (w), 2871 (m), 2962 (s). Zero-field ^{57}Fe Mössbauer [90 K]: δ = 0.45 mm/s, $|\Delta E_Q|$ = 0.62 mm/s, η = 0.573.

Synthesis of [$Fe_4Br(N{=}C^tBu_2)_5$] (2). To a stirring, deep red solution of **1** (0.103 g, 0.109 mmol) in THF (4.5 mL) at room temperature was added dropwise a yellow solution of Na($N{=}C^tBu_2$) (0.018 g, 0.110 mmol) in THF (3 mL). After 20 h, the volatiles were removed *in vacuo* to provide a black solid. This solid was triturated with pentane (3 × 1 mL), extracted with pentane (6 mL), and filtered through a Celite column supported on glass wool (0.5 cm × 5 cm). The filtrate was concentrated *in vacuo*. Storage of this vial at -25 °C for 48 h resulted in the deposition of solid dark purple crystalline material, which was isolated by decanting the supernatant (54 mg, 49% yield). X-ray quality crystals were grown by storage of Et_2O/acetonitrile solution of **2** (3 mL:0.5 mL) at -25 °C for 12 h. Anal. Calcd for $C_{45}H_{90}BrFe_4N_5$: C 53.81, H 9.03, N 6.97%. Found: C 53.49, H 8.99, N 6.97%. ^{1}H NMR (400 MHz, 25 °C, C_6D_6): δ 98.3 (br s, 72 H), 79.2 (br s, 18 H). ESI-MS: *m/z* 1003.3074 [M$^+$] (Calcd *m/z* 1003.3762). UV-vis/NIR (THF, 0.10 mM, 25 °C, L mol^{-1} cm^{-1}): 506 nm (ε = 4700), 923 nm (ε = 1100). FT-IR (KBr pellet, cm^{-1}): 584 (m), 644 (s), 765 (m), 842 (w), 877 (w), 973 (m), 1035 (w), 1192 (s), 1224 (m), 1240 (m), 1369 (s), 1373 (m), 1461

(m), 1481 (s), 1539 (w), 1602 (s), 1666 (m), 2233 (w), 2875 (m), 2964 (s). Zero-field ^{57}Fe Mössbauer [90 K]: δ = 0.45 mm/s, $|\Delta E_Q|$ = 0.39 mm/s, η = 0.558; δ = 0.59 mm/s, $|\Delta E_Q|$ = 1.14 mm/s, η = 0.600.

Associated Content

Supporting Information

The supporting information is available free of charge at https://pubs.acs.org.

- Experimental procedures and crystallographic, spectroscopic, and magnetic characterization details for **1** and **2** (PDF).

Author Information

Corresponding Author

Trevor W. Hayton – *Department of Chemistry and Biochemistry, University of California Santa Barbara, CA 93106, United States;* Email: hayton@chem.ucsb.edu

Authors

Phoebe R. Hertler – *Department of Chemistry and Biochemistry, University of California Santa Barbara, CA 93106, United States*

Linus Kautzsch – *Materials Department and Materials Research Laboratory, University of California, Santa Barbara, CA 93106, United States*

Alexander J. Touchton – *Department of Chemistry and Biochemistry, University of California Santa Barbara, CA 93106, United States*

Guang Wu – *Department of Chemistry and Biochemistry, University of California Santa Barbara, CA 93106, United States*

Notes

The authors declare no competing financial interest.

Acknowledgements

We thank the National Science Foundation (CHE 1764345) for financial support of this work. This research made use of a 400 MHz NMR spectrometer supported in part by NIH Shared Instrumentation Grant, S10OD012077. The MRL Shared Experimental Facilities are supported by the MRSEC Program of the National Science Foundation under award NSF DMR 1720256, a member of the NSF-funded Materials Research Facilities Network. Mössbauer spectra were collected with the help of Mr. Zongheng Wang. P.R.H. thanks the UCSB Eddleman Center for Quantum Innovation for a Graduate Student Support Grant.

References

(1) Zabala-Lekuona, A.; Seco, J. M.; Colacio, E. Single-Molecule Magnets: From Mn_{12}-Ac to Dysprosium Metallocenes, a Travel in Time. *Coord. Chem. Rev.* **2021**, *441*, 213984. https://doi.org/10.1016/J.CCR.2021.213984.

(2) Chakarawet, K.; Atanasov, M.; Marbey, J.; Bunting, P. C.; Neese, F.; Hill, S.; Long, J. R. Strong Electronic and Magnetic Coupling in M_4 (M = Ni, Cu) Clusters via Direct Orbital Interactions between Low-Coordinate Metal Centers. *J. Am. Chem. Soc* **2020**, *142* (45). https://doi.org/10.1021/jacs.0c08460.

(3) Nehrkorn, J.; Greer, S. M.; Malbrecht, B. J.; Anderton, K. J.; Aliabadi, A.; Krzystek, J.; Schnegg, A.; Holldack, K.; Herrmann, C.; Betley, T. A.; Stoll, S.; Hill, S. Spectroscopic Investigation of a Metal-Metal-Bonded Fe_6 Single-Molecule Magnet with an Isolated S = 19/2 Giant-Spin Ground State. *Inorg. Chem.* **2021**, *60* (7), 4610–4622. https://doi.org/10.1021/ACS.INORGCHEM.0C03595/.

(4) Toniolo, D.; Scopelliti, R.; Zivkovic, I.; Mazzanti, M. Assembly of High-Spin [Fe_3] Clusters by Ligand-Based Multielectron Reduction. *J. Am. Chem. Soc.* **2020**, *142* (16), 7301–7305. https://doi.org/10.1021/jacs.0c01664.

(5) Greer, S. M.; Gramigna, K. M.; Thomas, C. M.; Stoian, S. A.; Hill, S. Insights into Molecular Magnetism in Metal-Metal Bonded Systems as Revealed by a Spectroscopic and Computational Analysis of Diiron Complexes. *Inorg. Chem.* **2020**, *59* (24), 18141–18155. https://doi.org/10.1021/ACS.INORGCHEM.0C02605/.

(6) Hernández Sánchez, R.; Bartholomew, A. K.; Powers, T. M.; Ménard, G.; Betley, T. A. Maximizing Electron Exchange in a [Fe_3] Cluster. *J. Am. Chem. Soc.* **2016**, *138* (7), 2235–2243. https://doi.org/10.1021/jacs.5b12181.

(7) Sánchez, R. H.; Betley, T. A. Thermally Persistent High-Spin Ground States in Octahedral Iron Clusters. *J. Am. Chem. Soc.* **2018**, *140* (48), 16792–16806. https://doi.org/10.1021/jacs.8b10181.

(8) Hernández Sánchez, R.; Betley, T. A. Meta-Atom Behavior in Clusters Revealing Large Spin Ground States. *J. Am. Chem. Soc.* **2015**, *137* (43), 13949–13956. https://doi.org/10.1021/jacs.5b08962.

(9) Zhao, Q.; Harris, T. D.; Betley, T. A. $[(HL)_2Fe_6\,(NCMe)_m]^{n+}$ (m = 0, 2, 4, 6; n = -1, 0, 1, 2, 3, 4, 6): An Electron-Transfer Series Featuring Octahedral Fe_6 Clusters Supported by a Hexaamide Ligand Platform. *J. Am. Chem. Soc.* **2011**, *133* (21), 8293–8306. https://doi.org/10.1021/ja2015845.

(10) Hernández Sánchez, R.; Zheng, S. L.; Betley, T. A. Ligand Field Strength Mediates Electron Delocalization in Octahedral $[(HL)_2Fe_6(L')_m]^{n+}$ Clusters. *J. Am. Chem. Soc.* **2015**, *137* (34), 11126–11143. https://doi.org/10.1021/JACS.5B06453/.

(11) Sánchez, R. H.; Willis, A. M.; Zheng, S. L.; Betley, T. A. Synthesis of Well-Defined Bicapped-Octahedral Iron Clusters $[(^{tren}L)_2Fe_8(PMe_2Ph)_2]^n$ (n = 0, −1). *Angew. Chem. Int. Ed. Engl.* **2015**, *54* (41), 12009–12013. https://doi.org/10.1002/ANIE.201505671.

(12) Chakarawet, K.; Bunting, P. C.; Long, J. R. Large Anisotropy Barrier in a Tetranuclear Single-Molecule Magnet Featuring Low-Coordinate Cobalt Centers. *J. Am. Chem. Soc.* **2018**, *140* (6), 2058–2061. https://doi.org/10.1021/JACS.7B13394.

(13) Cook, A. W.; Bocarsly, J. D.; Lewis, R. A.; Touchton, A. J.; Morochnik, S.; Hayton, T. W. An Iron Ketimide Single-Molecule Magnet $[Fe_4\,(N{=}CPh_2)_6]$ with Suppressed through-Barrier Relaxation. *Chem. Sci.* **2020**, *11*, 4753–4757. https://doi.org/10.1039/d0sc01578d.

(14) Lippert, K. A.; Mukherjee, C.; Broschinski, J. P.; Lippert, Y.; Walleck, S.; Stammler, A.; Bögge, H.; Schnack, J.; Glaser, T. Suppression of Magnetic Quantum Tunneling in a Chiral Single-Molecule Magnet by Ferromagnetic Interactions. *Inorg. Chem.* **2017**, *56* (24), 15119–15129. https://doi.org/10.1021/ACS.INORGCHEM.7B02453/.

(15) Demir, S.; Jeon, I. R.; Long, J. R.; Harris, T. D. Radical Ligand-Containing Single-Molecule Magnets. *Coord. Chem. Rev.* **2015**, *289–290* (1), 149–176. https://doi.org/10.1016/J.CCR.2014.10.012.

(16) Glaser, T.; Hoeke, V.; Gieb, K.; Schnack, J.; Schröder, C.; Müller, P. Quantum Tunneling of the Magnetization in $[Mn^{III}_6M]^{3+}$ ($M = Cr^{III}$, Mn^{III}) SMMs: Impact of Molecular and Crystal Symmetry. *Coord. Chem. Rev.* **2015**, *289–290* (1), 261–278. https://doi.org/10.1016/J.CCR.2014.12.001.

(17) Gatteschi, D.; Sessoli, R.; Sessoli, R.; Gatteschi, D. Quantum Tunneling of Magnetization and Related Phenomena in Molecular Materials. *Angew. Chemie Int. Ed.* **2003**, *42* (3), 268–297. https://doi.org/10.1002/ANIE.200390099.

(18) Eames, E. V.; Harris, T. D.; Betley, T. A. Modulation of Magnetic Behavior via Ligand-Field Effects in the Trigonal Clusters $(^{Ph}L)Fe_3L^*_3$ (L* = Thf, Py, PMe_2Ph). *Chem. Sci.* **2012**, *3* (2), 407–415. https://doi.org/10.1039/C1SC00492A.

(19) Nicolini, A.; Affronte, M.; Santalucia, D. J.; Borsari, M.; Cahier, B.; Caleffi, M.; Ranieri, A.; Berry, J. F.; Cornia, A. Tetrairon(II) Extended Metal Atom Chains as Single-Molecule Magnets. *Dalt. Trans.* **2021**, *50* (22), 7571–7589. https://doi.org/10.1039/D1DT01007G.

(20) Nicolini, A.; Galavotti, R.; Barra, A. L.; Borsari, M.; Caleffi, M.; Luo, G.; Novitchi, G.; Park, K.; Ranieri, A.; Rigamonti, L.; Roncaglia, F.; Train, C.; Cornia, A. Filling the Gap in Extended Metal Atom Chains: Ferromagnetic Interactions in a Tetrairon(II) String Supported by Oligo-α-Pyridylamido Ligands. *Inorg. Chem.* **2018**, *57* (9), 5438–5448. https://doi.org/10.1021/ACS.INORGCHEM.8B00405/.

(21) Srinivasan, A.; Musgrave, R. A.; Rouzières, M.; Clérac, R.; McGrady, J. E.; Hillard, E. A. A Linear Metal–Metal Bonded Tri-Iron Single-Molecule Magnet. *Chem. Commun.* **2021**, *57* (98), 13357–13360. https://doi.org/10.1039/D1CC05043E.

(22) Zall, C. M.; Zherebetskyy, D.; Dzubak, A. L.; Bill, E.; Gagliardi, L.; Lu, C. C. A Combined Spectroscopic and Computational Study of a High-Spin S = 7/2 Diiron Complex with a Short Iron-Iron Bond. *Inorg. Chem.* **2012**, *51* (1), 728–736. https://doi.org/10.1021/ic202384b.

(23) Cotton, F. A.; Daniels, L. M.; Matonic, J. H.; Murillo, C. A. Highly Distorted Diiron(II, II) Complexes Containing Four Amidinate Ligands. A Long and Short Metal-Metal Distance. *Inorganica Chim. Acta* **1997**, *256* (2), 277–282. https://doi.org/10.1016/S0020-1693(96)05470-9.

(24) Cotton, F. A.; Daniels, L. M.; Falvello, L. R.; Matonic, J. H.; Murillo, C. A. Trigonal-Lantern Dinuclear Compounds of Diiron(I,II): The Synthesis and Characterization of Two Highly Paramagnetic $Fe_2(Amidinato)_3$ Species with Short Metal-Metal Bonds. *Inorganica Chim. Acta* **1997**, *256* (2), 269–275. https://doi.org/10.1016/S0020-1693(96)05469-2.

(25) Cotton, F. A.; Daniels, L. M.; Falvello, L. R.; Murillo, C. A. A New Class of Dinuclear Compounds: The Synthesis and x-Ray Structural Characterization of Tris(μ-Diphenyl-Formamidinato) Diiron. *Inorganica Chim. Acta* **1994**, *219* (1–2), 7–10. https://doi.org/10.1016/0020-1693(94)03832-5.

(26) Soriaga, R. A. D.; Javed, S.; Hoffman, D. M. Synthesis of Copper(I) Complexes with Ketimide and Hydrazide Ligands. *J. Clust. Sci.* **2010**, *21* (3), 567–575.

https://doi.org/10.1007/S10876-010-0343-5/.
(27) Cook, A. W.; Hrobárik, P. H.; Damon, P. L.; Wu, G.; Hayton, T. W. A Ketimide-Stabilized Palladium Nanocluster with a Hexagonal Aromatic Pd_7 Core. **2020**, *59* (2), 1471–1480. https://doi.org/10.1021/acs.inorgchem.9b03276.
(28) Lewis, R. A.; Morochnik, S.; Chapovetsky, A.; Wu, G.; Hayton, T. W. Synthesis and Characterization of $[M_2(N{=}C^tBu_2)_5]^-$ (M=Mn, Fe, Co): Metal Ketimide Complexes with Strong Metal-Metal Interactions. *Angew. Chemie Int. Ed.* **2012**, *51* (51), 12772–12775. https://doi.org/10.1002/anie.201206790.
(29) Kent, G. T.; Cook, A. W.; Damon, P. L.; Lewis, R. A.; Wu, G.; Hayton, T. W. Synthesis and Characterization of Two "Tied-Back" Lithium Ketimides and Isolation of a Ketimide-Bridged $[Cr_2]^{6+}$ Dimer with Strong Antiferromagnetic Coupling. *Inorg. Chem.* **2021**, *60* (7), 4996–5004. https://doi.org/10.1021/ACS.INORGCHEM.1C00052/.
(30) Eisenhart, R. J.; Rudd, P. A.; Planas, N.; Boyce, D. W.; Carlson, R. K.; Tolman, W. B.; Bill, E.; Gagliardi, L.; Lu, C. C. Pushing the Limits of Delta Bonding in Metal-Chromium Complexes with Redox Changes and Metal Swapping. *Inorg. Chem.* **2015**, *54* (15), 7579–7592. https://doi.org/10.1021/acs.inorgchem.5b01163.
(31) Pauling, L. Atomic Radii and Interatomic Distances in Metals. *J. Am. Chem. Soc.* **1947**, *69* (3), 542–553. https://doi.org/10.1021/JA01195A024/.
(32) Carpenter, S. H.; Baker, T. M.; Muñoz, S. B.; Brennessel, W. W.; Neidig, M. L. Multinuclear Iron-Phenyl Species in Reactions of Simple Iron Salts with PhMgBr: Identification of $Fe_4(\mu\text{-}Ph)_6(THF)_4$ as a Key Reactive Species for Cross-Coupling Catalysis. *Chem. Sci.* **2018**, *9* (41), 7931–7939. https://doi.org/10.1039/c8sc02915f.
(33) Lewis, R. A.; Wu, G.; Hayton, T. W. Synthesis and Characterization of an Iron(IV) Ketimide Complex. *J. Am. Chem. Soc.* **2010**, *132* (37), 12814–12816. https://doi.org/10.1021/ja104934n.
(34) Salvador B. M., I.; Daifuku, S. L.; Brennessel, W. W.; Neidig, M. L. Isolation, Characterization, and Reactivity of $Fe_8Me_{12}^-$: Kochi's S = 1/2 Species in Iron-Catalyzed Cross-Couplings with MeMgBr and Ferric Salts. *J. Am. Chem. Soc.* **2016**, *138* (24), 7492–7495. https://doi.org/10.1021/JACS.6B03760.
(35) Day, P.; Hush, N. S.; Clark, R. J. H. Mixed Valence: Origins and Developments. *Philos. Trans. R. Soc. A Math. Phys. Eng. Sci.* **2007**, *366* (1862), 5–14. https://doi.org/10.1098/RSTA.2007.2135.
(36) Robin, M. B.; Day, P. Mixed Valence Chemistry-A Survey and Classification. *Adv. Inorg. Chem. Radiochem.* **1968**, *10*, 247–422. https://doi.org/10.1016/S0065-2792(08)60179-X.
(37) D'alessandro, D. M.; Keene, F. R. Current Trends and Future Challenges in the Experimental, Theoretical and Computational Analysis of Intervalence Charge Transfer (IVCT) Transitions. *Chem. Soc. Rev.* **2006**, *35* (5), 424–440. https://doi.org/10.1039/B514590M.
(38) Lee, D.; DuBois, J. L.; Pierce, B.; Hedman, B.; Hodgson, K. O.; Hendrich, M. P.; Lippard, S. J. Structural and Spectroscopic Studies of Valence-Delocalized Diiron(II,III) Complexes Supported by Carboxylate-Only Bridging Ligands. *Inorg. Chem.* **2002**, *41* (12), 3172–3182. https://doi.org/10.1021/IC011050N.
(39) Lee, D.; Krebs, C.; Huynh, B. H.; Hendrich, M. P.; Lippard, S. J. Valence-Delocalized Diiron(II,III) Cores Supported by Carboxylate-Only Bridging Ligands. *J. Am. Chem. Soc.* **2000**, *122* (20), 5000–5001. https://doi.org/10.1021/JA994448F.
(40) Chilton, N. F.; Anderson, R. P.; Turner, L. D.; Soncini, A.; Murray, K. S. PHI: A

Powerful New Program for the Analysis of Anisotropic Monomeric and Exchange-Coupled Polynuclear d- and f-Block Complexes. *J. Comput. Chem.* **2013**, *34* (13), 1164–1175. https://doi.org/10.1002/JCC.23234.

(41) Gould, C. A.; Randall McClain, K.; Reta, D.; C Kragskow, J. G.; Marchiori, D. A.; Lachman, E.; Choi, E.-S.; Analytis, J. G.; David Britt, R.; Chilton, N. F.; Harvey, B. G.; Long, J. R. Ultrahard Magnetism from Mixed-Valence Dilanthanide Complexes with Metal-Metal Bonding. *Science.* **2022**, *375* (6577), 198–202. https://doi.org/10.1126/science.abl5470.

(42) Clegg, W.; Snaith, R.; Shearer, H. M.; Wade, K.; Whitehead, G. Azomethine Derivatives. Part 20. Crystal and Molecular Structures of the Lithioketimine $[\{Li(N{=}C^tBu_2)\}_6]$ and Lithioguanidine $[\{Li[N{=}C(NMe_2)_2]\}_6]$; Electron-Deficient Bridging of Li_3 Triangles by Methyleneamino-Nitrogen Atoms. *Dalt. Trans.* **1983**, 1309–1317. https://doi.org/10.1039/dt9830001309.

(43) Bain, G. A.; Berry, J. F. Diamagnetic Corrections and Pascal's Constants. *J. Chem. Educ.* **2008**, *85* (4), 532–536. https://doi.org/10.1021/ED085P532.

Table of Contents Graphic

The $[Fe_4]^{6+}$-containing clusters, $[Fe_4Br_2(N{=}C^tBu_2)_4]$ and $[Fe_4Br(N{=}C^tBu_2)_5]$, feature $S = 7$ ground states and zero-field relaxation barriers of $U_{eff} \approx 14$ cm^{-1}.